Detection of a supervoid aligned with the cold spot of the cosmic microwave background

István Szapudi,[1][*] András Kovács,[2,3,4] Benjamin R. Granett,[5] Zsolt Frei,[2,3]
Joseph Silk,[6] Will Burgett,[1] Shaun Cole,[7] Peter W. Draper,[7] Daniel J. Farrow,[7]
Nicholas Kaiser,[1] Eugene A. Magnier,[1] Nigel Metcalfe,[7] Jeffrey S. Morgan,[1]
Paul Price,[8] John Tonry[1] and Richard Wainscoat[1]

[1]*Institute for Astronomy, University of Hawaii 2680 Woodlawn Drive, Honolulu, HI 96822, USA*
[2]*Institute of Physics, Eötvös Loránd University, Pázmány Péter sétány 1/A, 1117 Budapest, Hungary*
[3]*MTA-ELTE EIRSA 'Lendület' Astrophysics Research Group, Pázmány Péter sétány 1/A, 1117 Budapest, Hungary*
[4]*Institut de Física d'Altes Energies, Universitat Autónoma de Barcelona, E-08193 Bellaterra (Barcelona), Spain*
[5]*INAF OA Brera, Via E. Bianchi 46, I-23807 Merate, Italy*
[6]*Department of Physics and Astronomy, The Johns Hopkins University, Baltimore, MD 21218, USA*
[7]*Department of Physics, Durham University, South Road, Durham DH1 3LE, UK*
[8]*Department of Astrophysical Sciences, Princeton University, Princeton, NJ 08544, USA*

ABSTRACT

We use the *WISE*-2MASS infrared galaxy catalogue matched with Pan-STARRS1 (PS1) galaxies to search for a supervoid in the direction of the cosmic microwave background (CMB) cold spot (CS). Our imaging catalogue has median redshift $z \simeq 0.14$, and we obtain photometric redshifts from PS1 optical colours to create a tomographic map of the galaxy distribution. The radial profile centred on the CS shows a large low-density region, extending over tens of degrees. Motivated by previous CMB results, we test for underdensities within two angular radii, $5°$, and $15°$. The counts in photometric redshift bins show significantly low densities at high detection significance, $\gtrsim 5\sigma$ and $\gtrsim 6\sigma$, respectively, for the two fiducial radii. The line-of-sight position of the deepest region of the void is $z \simeq 0.15$–0.25. Our data, combined with an earlier measurement by Granett, Szapudi & Neyrinck, are consistent with a large $R_{\rm void} = (220 \pm 50)\, h^{-1}$ Mpc supervoid with $\delta_m \simeq -0.14 \pm 0.04$ centred at $z = 0.22 \pm 0.03$. Such a supervoid, constituting at least a $\simeq 3.3\sigma$ fluctuation in a Gaussian distribution of the Λ cold dark matter model, is a plausible cause for the CS.

Key words: surveys – cosmic background radiation – cosmology: observations – large-scale structure of Universe.

1 INTRODUCTION

The cold spot (CS) of the cosmic microwave background (CMB) is an exceptionally cold $-70\,\mu\rm K$ area centred on $(l, b) \simeq (209°, -57°)$ Galactic coordinates. It was first detected in the *Wilkinson Microwave Anisotropy Probe* (Bennett et al. 2013) maps at $\simeq 3\sigma$ significance using wavelet filtering (Vielva et al. 2004; Cruz et al. 2005). The CS is perhaps the most significant among the 'anomalies', potential departures from isotropic and/or Gaussian statistics, and all confirmed by *Planck* (Planck Collaboration XXIII 2014). Explanations of the CS range from statistical fluke through hitherto undiscovered physics, e.g. textures (Cruz et al. 2008; Vielva 2010), to the linear and non-linear ISW effect (Sachs & Wolfe 1967; Rees & Sciama 1968) from a $\gtrsim 200\, h^{-1}$ Mpc supervoid centred on the

CS (Inoue & Silk 2006, 2007; Inoue, Sakai & Tomita 2010). The latter would be readily detectable in large-scale structure surveys thus motivating several observational studies.

A low-density region approximately aligned with the CS was detected in a catalogue of radio galaxies (Rudnick, Brown & Williams 2007), although its significance has been disputed (Smith & Huterer 2010). A targeted redshift survey in the area (Bremer et al. 2010) found no evidence for a void in the redshift range of $0.35 < z < 1$, while an imaging survey with photometric redshifts (Granett, Szapudi & Neyrinck 2010) excluded the presence of a large underdensity of $\delta \simeq -0.3$ between redshifts of $0.5 < z < 0.9$ and finding none at $0.3 < z < 0.5$. Both of these surveys ran out of volume at low redshifts due to their small survey area, although the data are consistent with the presence of a void at $z < 0.3$ with low significance (Granett et al. 2010). In a shallow photometric redshift catalogue constructed from the Two Micron All Sky Survey (2MASS; Skrutskie et al. 2006) and SuperCOSMOS (Hambly et al.
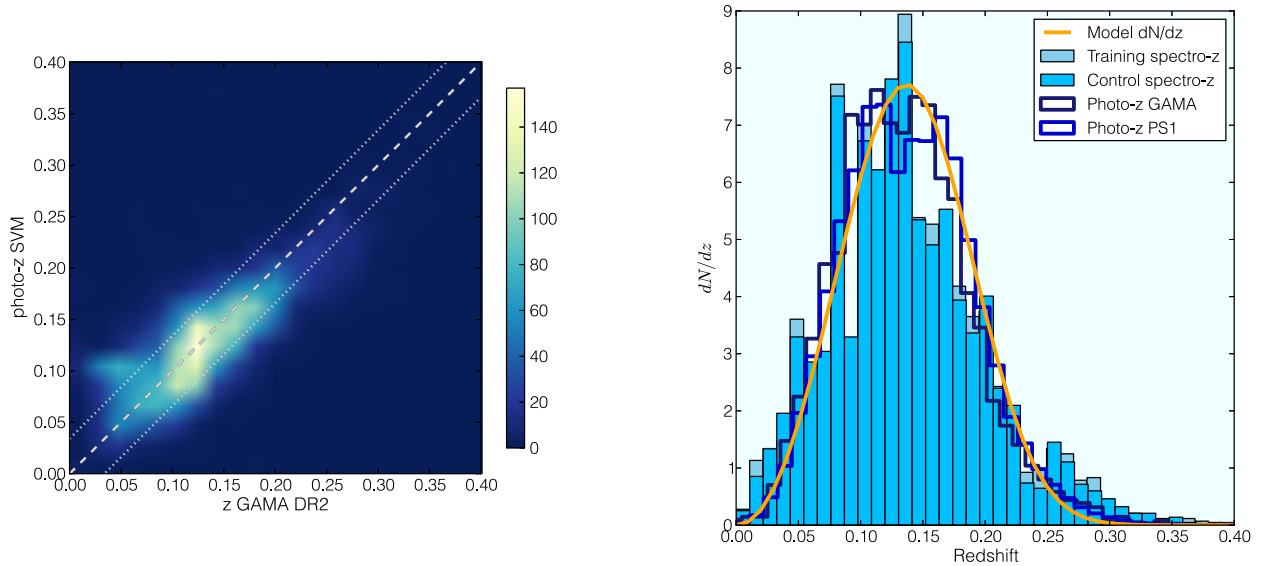
[*] E-mail: szapudi@ifa.hawaii.edu

Figure 1. The left-hand panel shows the photo-*z* accuracy achieved by the SVM. Dotted lines indicate the $\sigma_z \approx 0.034$ 1σ error bars around the expectation. The right-hand panel illustrates the normalized redshift distributions of our subsamples used in the photo-*z* pipeline: training and control sets selected in GAMA, photo-*z* distributions estimated for the *WISE*-2MASS-PS1-GAMA control sample, and photo-*z*s of interest in the *WISE*-2MASS-PS1 matched area. The median redshift of all subsamples is $z \simeq 0.14$.

2001) with a median redshift of $z = 0.08$ an underdensity was found (Francis & Peacock 2010) that can account for a CMB decrement of $\Delta T \simeq -7\,\mu\mathrm{K}$ in the standard Λ cold dark matter (ΛCDM) cosmology. While so far no void was found that could fully explain the CS, there is strong, $\gtrsim 4.4\sigma$, statistical evidence that superstructures imprint on the CMB as cold and hot spots (Granett, Neyrinck & Szapudi 2008, 2009; Pápai & Szapudi 2010; Cai et al. 2014; Planck Collaboration XXIII 2014). Note that the imprinted temperature in all of these studies is significantly colder than simple estimates from linear ISW (e.g. Rudnick et al. 2007; Pápai & Szapudi 2010; Pápai, Szapudi & Granett 2011) would suggest.

The *Wide-field Infrared Survey Explorer* (*WISE*; Wright et al. 2010) all-sky survey effectively probes low redshift $z \leq 0.3$ unconstrained by previous studies. Using the *WISE*-2MASS all sky galaxy map of Kovács & Szapudi (2015) as a base catalogue, we match a 1300 deg² area with the PV1.2 reprocessing of Pan-STARRS1 (hereafter PS1; Kaiser 2004), adding optical colours for each object. In the resulting catalogue with photometric redshifts we test for the presence of a large low-density region, a supervoid, centred on the CS. We defined the centre of the CS from the latest *Planck* results (Planck Collaboration XXIV 2014). Based on the literature, we decided in advance to test for an underdensity at 5° (Vielva et al. 2004; Cruz et al. 2005; Rudnick et al. 2007; Bremer et al. 2010; Granett et al. 2010) and 15° (Inoue et al. 2010; Zhang & Huterer 2010) of radii. The fact that these values gleaned from CMB independently of our (large-scale structure) data simplifies the interpretation of our results in the Bayesian framework, in particular, minimize any a posteriori bias.

The paper is organized as follows. Data sets and map-making algorithms are described in Section 2; our observational results are presented in Section 3; the final section contains a summary, discussion, and interpretation of our results.

2 DATA SETS AND METHODOLOGY

Initially, we select galaxies from the *WISE*-2MASS catalogue (Kovács & Szapudi 2015) containing sources to flux limits of

$W1_{\mathrm{WISE}} \leq 15.2$ mag and $W1_{\mathrm{WISE}} - J_{2\mathrm{MASS}} \leq -1.7$. We add a further limit of $J_{2\mathrm{MASS}} \leq 16.5$ mag to ensure spatial homogeneity based on our experiments. This refinement shifts the median redshift of the sample to $z \simeq 0.14$. The catalogue covers 21 200 deg² after masking. We mask pixels with $E(B - V) \geq 0.1$, and regions at galactic latitudes $|b| < 20°$ to exclude potentially contaminated regions near the Galactic plane (Schlegel, Finkbeiner & Davis 1998). These conservative limits result in a data set deeper than the 2MASS Extended Source Catalog (Jarrett et al. 2000) and more uniform than *WISE* (Kovács et al. 2013). These galaxies have been matched with PS1 objects within a $50° \times 50°$ area centred on the CS, except for a Dec. ≥ -28.0 cut to conform to the PS1 boundary. We used PV1.2 reprocessing of PS1 in an area of 1300 deg².

For matching we applied a nearest neighbour search using the SCIPY kd-TREE algorithm with 1-arcsec matching radius, finding a PS1 pair for 86 per cent of the infrared galaxies, and resulting 73 100 objects in the final catalogue. Galaxies without a PS1 match are faint in the optical, and predominantly massive early-type galaxies at $z > 1$ (Yan et al. 2013). For PS1, we required a proper measurement of Kron (Kron 1980) and PSF magnitudes in g_{P1}, r_{P1}, and i_{P1} bands that were used to construct photometric redshifts (photo-*z*s) with a Support Vector Machine (SVM) algorithm, and the PYTHON SCIKIT-LEARN (Pedregosa et al. 2011) routines in regression mode. The training and control sets were created matching *WISE*-2MASS, PS1, and the Galaxy and Mass Assembly (GAMA; Driver et al. 2011) redshift survey. We chose a Gaussian kernel for our SVM and trained on 80 per cent of the GAMA redshifts, while the rest were used for a control set. We empirically tuned the standard SVM parameters, finding the best performance when using $C = 10.0$, and $\gamma = 0.1$. We characterize our photo-*z* quality with the error $\sigma_z = \sqrt{\langle(z_{\mathrm{phot}} - z_{\mathrm{spec}})^2\rangle}$, finding $\sigma_z \approx 0.034$, as summarized in Fig. 1.

3 RESULTS

The projected *WISE*-2MASS galaxy density field along with the *Planck* Spectral Matching Independent Component Analysis
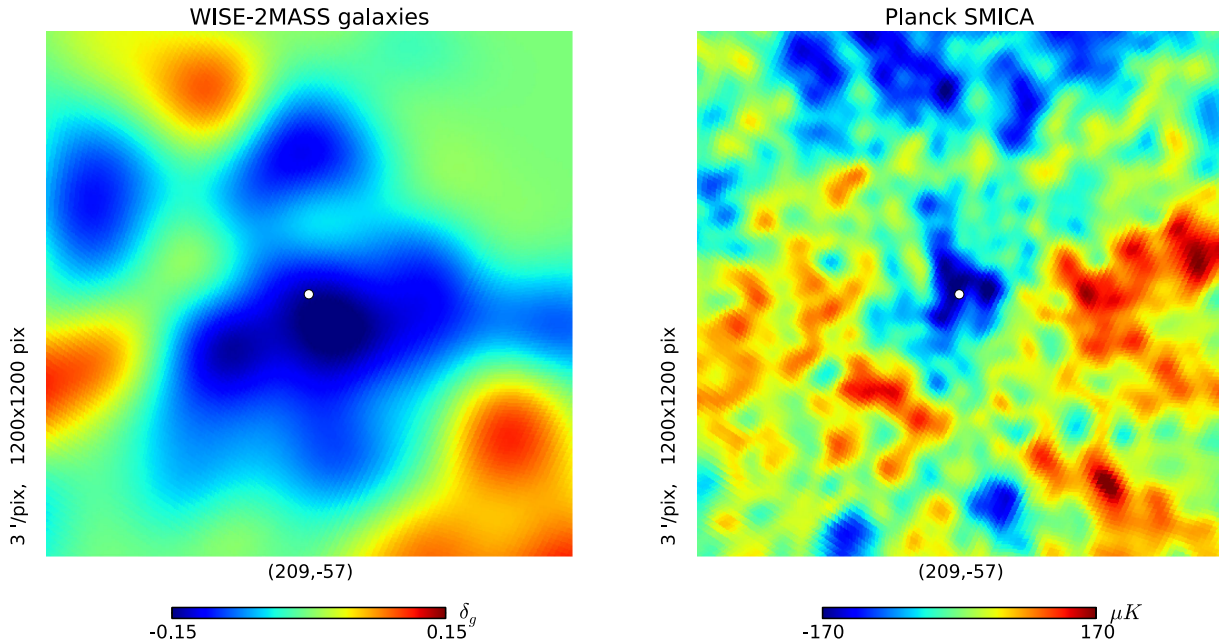
Figure 2. Gnomonic projections of the *WISE*-2MASS projected density map (left) and the *Planck* SMICA CMB map (right). Both maps were created at $N_{side} = 128$ resolution. We applied a Gaussian smoothing of $10°$ ($2°$) to the *WISE*-2MASS (*Planck* SMICA) map. White points indicate the centre of the image, that is the centre of the CS as defined in Planck Collaboration XXIII (2014) results.

(SMICA) CMB map are shown in Fig. 2. We have found that the most prominent large-scale underdensity found in *WISE*-2MASS is well aligned with the CS, although their sizes are different. Next we examine the radial statistics of this projected galaxy field, and apply photometric redshift techniques for a tomographic imaging of the region of interest. To avoid confusion, we will use the word 'significance' to denote the significance of the detection of an underdensity, while 'rarity' will denote the probability (expressed in σs) that the particular underdensity would appear in a cosmological random field.

3.1 Significance and rarity: 2D

We first study the CS region in projection, using the *WISE*-2MASS galaxies only. We measure radial galaxy density profiles in rings and discs centred on the CS in a bin size of $2.5°$, allowing identification of relatively small-scale structures. In Fig. 3, the dark shaded region represents Poisson fluctuations in our measurement in rings, calculated from the total number of galaxies in a ring. Fig. 3 shows a significant depression of sources. The size of the underdensity is surprisingly large: it is detected up to $\sim20°$ with high ($\gtrsim5\sigma$) detection significance. In addition, the profile has ring-like overdensity surrounding the CS region at large angular radii. This is consistent with a supervoid surrounded by a gentle compensation that converges to the average galaxy density at $\sim50°$ (see e.g. Pápai et al. 2011). At our predetermined radii, $5°$ and $15°$, we have a signal-to-noise ratio S/N ~ 12 for detecting the rings.

These results represent the detection significance of the underdensity calculated from Poisson errors. To quantify the cosmic rarity of the structure, we estimated the error bars arise from cosmic variance as well. Poisson fluctuations and cosmic variance errors are compared in Fig. 3, corresponding to dark and light shaded regions. We created 10 000 Gaussian simulations of the projected galaxy map using the HEALPIX SYNFAST routine. As an input, we used a theoretical angular power spectrum assuming flat ΛCDM cosmological
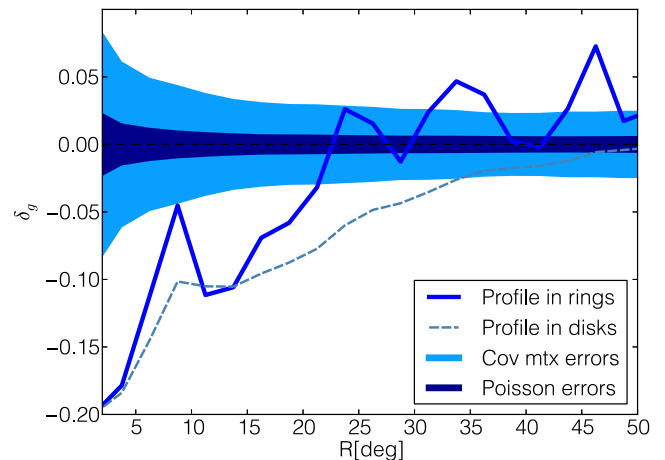

Figure 3. Radial galaxy density profile of the *WISE*-2MASS galaxy catalogue, centred on the CS. The underdensity is detected out to tens of degrees in radius, consistent with an $r \approx 200\,h^{-1}$ Mpc supervoid with $\delta_g \simeq -0.2$ deepening in its centre. Note that the deeper central region is surrounded by a denser shell.

model, and the redshift distribution of the *WISE*-2MASS sources. With the full covariance information, we evaluated a χ^2 statistic for our radial density profile measurement compared to zero value in each bin. We have found $\chi^2 = 43.94$ for 24 degrees-of-freedom (the number of radial bins), i.e. $p = 0.007$ or $\sim3\sigma$ characterizing the cosmic rarity of the supervoid in the (projected) concordance ΛCDM framework.

3.2 Significance: 3D

We use the *WISE*-2MASS-PS1 galaxy catalogue with photo-z information to constrain the position, size, and depth of supervoids. We count galaxies as a function of redshift in discs centred on the CS at
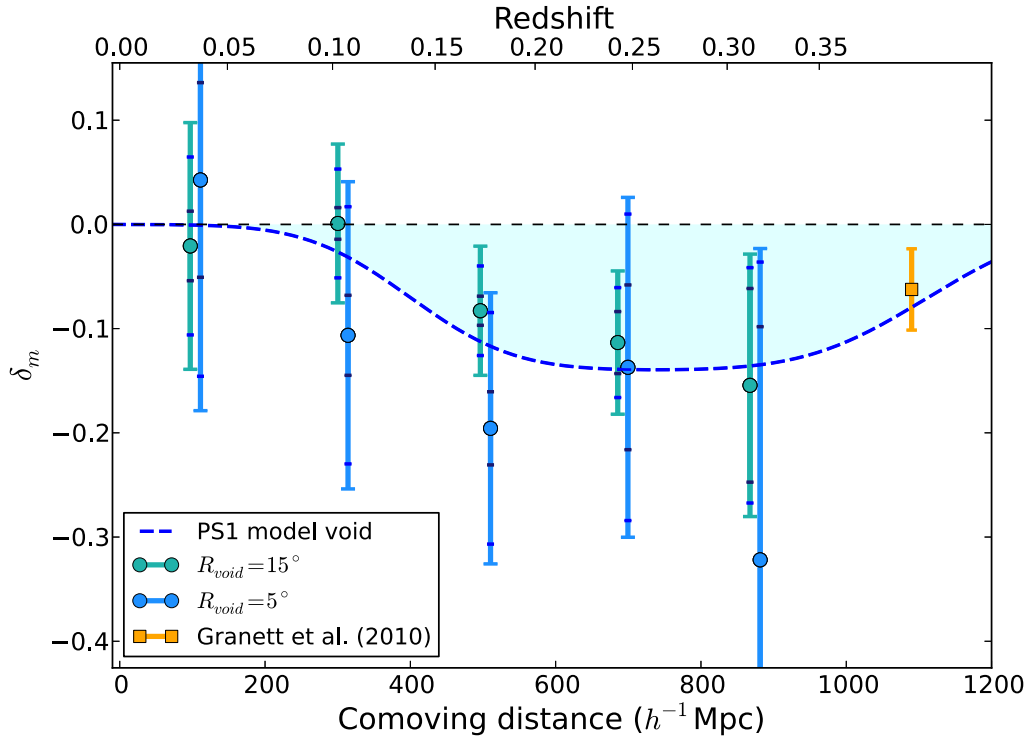
Figure 4. Our measurements of the matter density in the line of sight using the $\Delta z = 0.07$ photo-z bins we defined. We detected a significant depression in δ_m in $r = 5°$ and $15°$ test circles. We used our simple modelling tool to examine the effects of photo-z errors, and test the consistency of simple top-hat voids with our measurements. A data point by Granett et al (2010) accounts for the higher redshift part of the measurement. Dark blue (blue) stripes in error bars mark the contribution of Poisson (cosmic variance) fluctuations to the total error, while the additional part of the bars indicates the systematic effect of small survey coverage. See text for details.

our fiducial angular radii, $r = 5°$, and $15°$, and compare the results to the average redshift distribution of our sample. Since the latter discs are cut by the PS1 mask, we always use the available area, and compensate accordingly. We fit the observed redshift distribution with a model $dN/dz \propto e^{-(z/z_0)^\alpha} z^\beta$, estimating the parameters as $z_0 = 0.16$, $\alpha = 3.1$, and $\beta = 1.9$. The average redshift distribution was obtained by counting all galaxies within our catalogue outside the $15°$ test circle, i.e. using 750 deg^2, and errors of this measurement are propagated to our determination of the underdensity as follows. Our photo-z bins were of width $\Delta z = 0.07$, and we compared the galaxy counts inside the test circles to those of the control area. We added an extra bin from the measurement of Granett et al. (2010) centred at $z = 0.4$ in order to extend our analysis to higher redshifts in Fig. 4.

Assuming accurate knowledge of the average density, the detection significance has Poisson statistics. However, given the fact that our photo-z catalogue is less than a factor of 2 larger than the area enclosed within the $15°$ radius, we include error corresponding to the uncertainty of the average density due to Poisson and cosmic variance, as well as systematic errors. We estimate each term using simulations and the data.

In order to create simulations of the density field, we first estimated the bias of the galaxy distribution. We modelled the angular power spectrum of the *WISE*-2MASS galaxy density map using the PYTHON COSMOPY package,[1] and performed a measurement using SPICE (Szapudi, Prunet & Colombi 2001). We assumed concordance flat ΛCDM cosmological model with a fiducial value for the ampli-
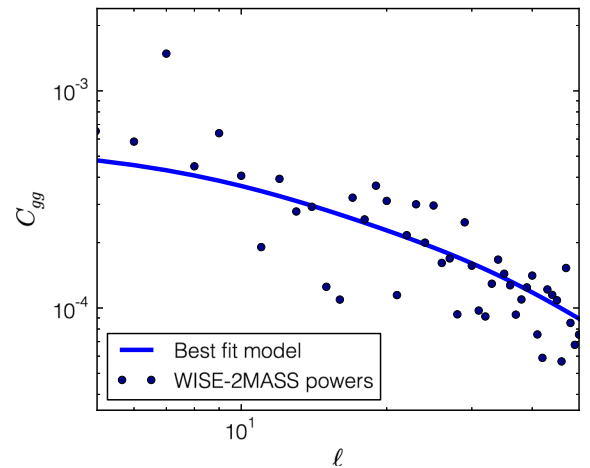
[1] http://www.ifa.hawaii.edu/cosmopy/

Figure 5. Measurement of the angular power spectrum of the *WISE*-2MASS galaxies is presented along with the best-fitting theoretical model from concordance ΛCDM cosmology, and a best-fitting model with bias $b_g = 1.41 \pm 0.07$. See text for details.

tude of fluctuations $\sigma_8 = 0.8$. Then we carried out a χ^2-based maximum likelihood parameter estimation, finding $b_g = 1.41 \pm 0.07$. The minimum value of $\chi^2_{\min} = 4.72$ is an excellent fit for $\nu = 7$ degrees-of-freedom of our fitting procedure (8 bins in the angular power spectrum shown in Fig. 5 and an amplitude parameter). This bias is comparable to earlier findings that measured the value of b_g for 2MASS selected galaxies (Rassat et al. 2007), despite the additional uncertainty due to that of σ_8. Using the bias, we

generated C_{gg} galaxy angular power spectra with COSMOPY for the five photo-z bins applying a sharp cut to the full redshift distribution. As before, we assumed the concordance flat ΛCDM cosmology. We then applied the same procedure as in Section 3.1 using SYNFAST for generating 1000 random HEALPIX simulations for each photo-z bin.

The cosmic variance affecting the average density from using a small patch on the sky is characterized by estimating the variance of differences in mean densities estimated in the PS1 area and in full sky. In addition, we estimated a systematic errors by comparing cosmic variance from simulations to the variance of the average density of small patches measured in PS1 data. The extra variance corresponds to systematic errors, and possibly to any (presumably small) inaccuracy of our concordance cosmology and bias models. The total error thus corresponds to the above three contributions shown in Fig. 4. The procedure was repeated for each photo-z bins. We compared mean densities estimated in the part of the PS1 area used for obtaining the average density, and those measured in $R = 5°$ and $15°$ circles.

Qualitatively, simulations at lower redshifts contain stronger fluctuations on large scales, as the input power spectra contain higher powers for low-ℓ. This effect is reflected in the systematic and cosmic variance error contributions we obtained, since the value of these corrections gradually decreases by ∼50 per cent from bin 1 to bin 5. See Fig. 4 for details.

Using the above determined error bars, we find S/N ∼ 5 and ∼6 for the deepest underdensity bins for $r = 5°$ and $15°$ characterizing our detection significance in 3D.

3.3 Top-hat supervoid model and rarity in 3D

To aid the interpretation of these results, we built toy models from top-hat voids in the z direction and modelled the smearing by the photo-z errors. The initial top-hat with three parameters, redshift (z_{void}), radius (R_{void}), and central depth (δ_m), was smoothed using the distribution corresponding to the photometric redshift errors. The model redshift distribution was then multiplied with this smeared profile.

The void model can be compared to observations using a χ^2-based maximum likelihood parameter estimation. We focus on the largest scale underdensity, therefore we only use the $r = 15°$ data, and replace our last bin with the measurement of Granett et al. (2010). This gives $n = 6$ bins with $k = 3$ parameters, thus the degrees of freedom are $\nu = n - k = 3$. We find a $\chi^2_{15°} = 7.74$ for the null hypothesis of no void. The best-fitting parameters with marginalized errors are $z_{void} = 0.22 \pm 0.03$, $R_{void} = (220 \pm 50)\,h^{-1}$ Mpc, and $\delta_m = -0.14 \pm 0.04$ with $\chi^2_{min} = 3.55$. Despite the simplicity of the toy model, the minimum chi-square indicates a good fit, expecting $\chi^2_{min} = \nu \pm \sqrt{2\nu}$. Nevertheless, more complexity is revealed by these counts, as bins 2–3 of the $r = 5°$ counts at redshifts $0.10 \leq z \leq 0.15$ evidence the deepening of the supervoid in the centre, or substructure. For accurate prediction of the effect on the CMB, the density field around the CS region, including any substructure needs to be mapped precisely. This is left for future work, although we present a preliminary tomographic imaging of the region next. Nevertheless, using the above parameters and errors, we estimate that an underdensity is at least 3.3σ rare in a ΛCDM model with $\sigma_8 \simeq 0.8$, integrating the power spectrum to obtain the variance at $220\,h^{-1}$ Mpc and using Gaussian statistics for the probability. To get a lower bound on the rarity of the void, we used the fit parameters within their 1σ range always in the sense to *increase* the likelihood of the underdensity in ΛCDM; thus the void we detected appears to be fairly rare. Nevertheless, the top-hat is an oversimplified toy model; thus the estimates based on it should be taken only as an initial attempt to interpret the detected supervoid in the concordance model framework.

3.4 Tomographic imaging

For three-dimensional impression of the galaxy distribution around the CS, we created maps in three photo-z slices with a width of $z < 0.09$, $0.11 < z < 0.14$, and $0.17 < z < 0.22$, and smoothed with a Gaussian at $2°$ scales. Then we overplot the *Planck* SMICA CMB map as contours in Fig. 6. The deepest part of the void appears to be close to the centre of the CS in the middle slice.

While photo-z errors do not allow a fine-grained interpretation of the results, we observe a complex structure of voids, possibly a deeper, smaller void nested in a larger, shallower supervoid, or the deepening of a supervoid profile towards the middle. The foreground overdensity apparent in the first picture, especially the 'filament' on the left-hand side running along the PS1 survey boundary further complicates the picture. It is likely to be foreground, since it is more significant in the shallowest slice, gradually fading out at higher z. These tomographic maps show a compensated surrounding overdense shell around the supervoid at $r \gtrsim 15°$, which plausibly would have fragmented into galaxy clusters visible in the projected slices as several 'hot spots' surrounding the CS region. Note that Gurzadyan et al. (2014) use K-map statistics to *Planck* to show that the CS has a morphological structure similar to a void.

4 DISCUSSION AND CONCLUSIONS

Using our *WISE*-2MASS-PS1 data set, we detected a low-density region, or supervoid, centred on the CS region: at $5°$ and $15°$ radii our detection significances are 5σ and 6σ, respectively. We measured the galaxy density as a function of redshift at the two predetermined radii. The galaxy underdensity is centred at $z \simeq 0.22$ for $15°$, and even deeper around $z \simeq 0.15$ for $5°$. The counts are consistent with a supervoid of size $R_{void} \simeq 220\,h^{-1}$ Mpc and average density $\delta_g \simeq -0.2$. It is noteworthy that this result is comparable to the local $300\,h^{-1}$ Mpc size underdensity claimed by Keenan et al. (2012) with $\delta_g \simeq -0.3$.

We estimated the true underdensity of the supervoid, by modelling the angular power spectrum of the *WISE*-2MASS galaxy density map, finding $b_g = 1.41 \pm 0.07$. The resulting underdensity in the dark matter field, therefore, is $\delta = \delta_g/b_g \simeq -0.14 \pm 0.04$ assuming a linear bias relation. Given the uncertainties of our toy model, we estimated that the supervoid we detected corresponds to a rare, at least 3.3σ, fluctuation in ΛCDM, although the 1σ range of our measurements is also consistent with a void very unlikely in concordance models. This agrees very well with our estimate that the underdensity found in the projected *WISE*-2MASS is a 3σ fluctuation compared to simple Gaussian simulations. Let's denote the probability of finding a CS on the CMB with p_{CS}, the probability of finding a void in LSS with p_{void}, and finally the probability of them being in alignment by chance with p_{match}. Let H_1 be the hypothesis, that the two structures are random fluctuations, and their alignment is random, and H_2 the hypothesis that the void is a random fluctuation *causing* the CS. The ratio of probabilities is $p_{H_2}/p_{H_1} = 1/(p_{CS}\,p_{match})$. For instance, conservatively, if the alignment is at the $\simeq 2°$ level and the rarity of the CS is only $\simeq 2\sigma$, the ratio still overwhelmingly favours H_2. Thus chance alignment of two rare objects is not plausible, and a causal relation between the CS and the supervoid is more likely by a factor of at least $\simeq 20\,000$.
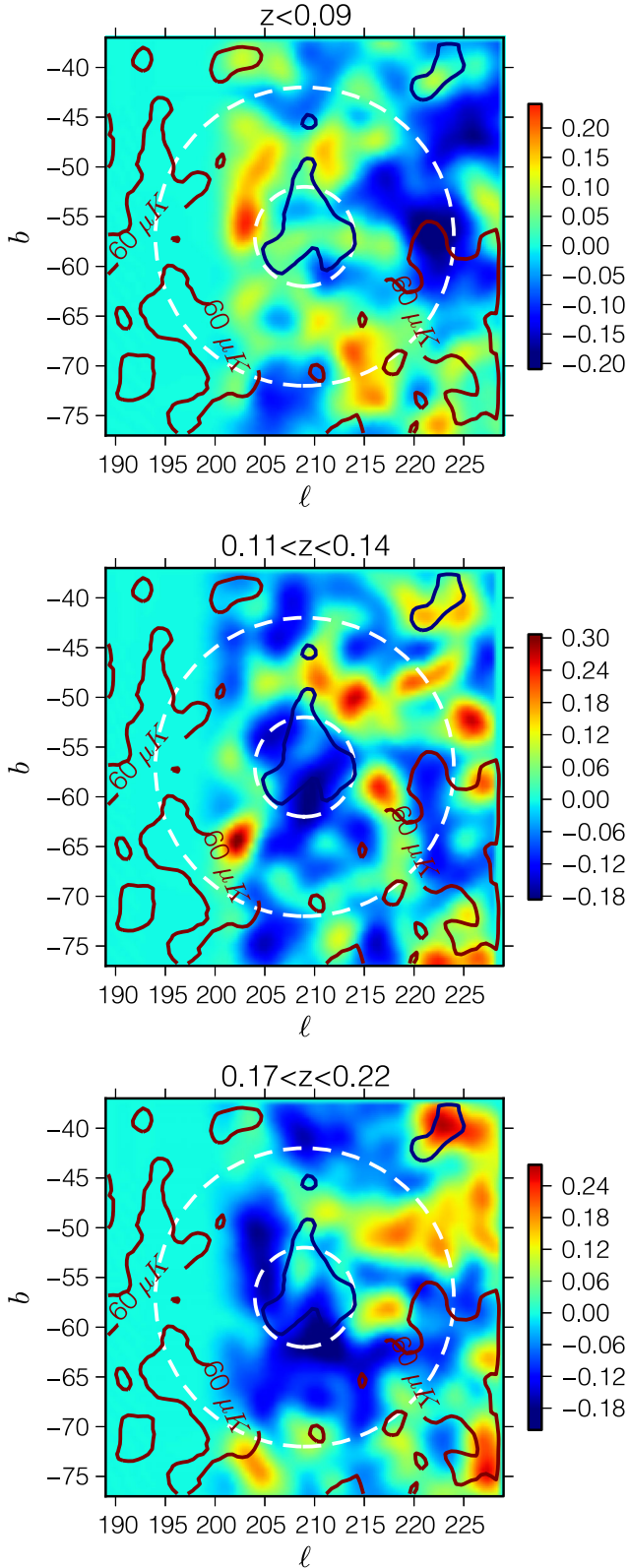
Using Rudnick et al. (2007), we estimate that the linear ISW effect of this supervoid is of order $-20\,\mu K$ on the CMB. The effect might be a factor or few higher if the size of the void is larger, if the compensation is taken into account (Pápai et al. 2011), and/or if non-linear and general relativistic effects are included (e.g. Inoue & Silk 2006, 2007). Most recently, Finelli et al. (in preparation) attempted to fit a non-linear LTB model (Garcia-Bellido & Haugbølle 2008) based on the projected profile in the *WISE*-2MASS catalogue, and find an effect not much larger than our initial estimate.

Superstructures affect several cosmological observables, such as CMB power spectrum and two and three point correlation functions (Masina & Notari 2009a, 2010), CMB lensing (Das & Spergel 2009; Masina & Notari 2009b), 21 cm lensing (Kovetz & Kamionkowski 2013), CMB polarization (Vielva et al. 2011), or cosmic radio dipole (Rubart, Bacon & Schwarz 2014), and even B-mode polarization (BICEP2 Collaboration 2014). Furthermore, the other CMB anomalies associated with large-angle correlations (Land & Magueijo 2005; Copi et al. 2006, 2013) should be revisited in light of these findings.

Our results suggest the connection between the supervoid and the CS, but further studies addressing the rarity of the observed supervoid observationally would be needed to firmly establish it. This needs a larger photometric redshift data set that will reach beyond $50°$ radius, such as PS1 with the second reprocessing thus improved calibration, and Dark Energy Survey (The Dark Energy Survey Collaboration 2005). As a first step, we smoothed the projected *WISE*-2MASS map with a $25°$ Gaussian, finding only one void as significant as the one we discovered in the CS region. This second void, to be followed up in future research and located near the constellation Draco, is clearly visible in the shallow 2MASS maps of Rassat, Starck & Dupé (2013), Francis & Peacock (2010) as a large underdensity, and in the corresponding reconstructed ISW map of Rassat & Starck (2013) as a cold imprint. Therefore the Draco supervoid is likely to be closer thus smaller in physical size. More accurate photometric redshifts, possibly with novel methods such as that of Ménard et al. (2013), will help us to constrain further the morphology and the size of the supervoids, and a deeper data set would constrain their extent redshift space. Any tension with ΛCDM, e.g. in the possible rarity of the observed supervoids, could be addressed in models of modified gravity, ordinarily screened in clusters, but resulting in an enhanced growth rate of voids as well as an additional contribution to the ISW signal.

ACKNOWLEDGEMENTS

Figure 6. Tomographic view of the CS region in δ_m. The top panel appears to show a foreground overdensity at the low redshift. A void is apparent at $0.11 < z < 0.14$ mostly inside the $5°$ central region of the CS. The large underdensity on the bottom panel at moderately higher redshifts may be slightly off centre with respect to the CS.

REFERENCES

Bennett C. L. et al., 2013, ApJS, 208, 20

BICEP2 Collaboration, 2014, Phys. Rev. Lett., 112, 241101

Bremer M. N., Silk J., Davies L. J. M., Lehnert M. D., 2010, MNRAS, 404, L69

Cai Y.-C., Neyrinck M. C., Szapudi I., Cole S., Frenk C. S., 2014, ApJ, 786, 110

Copi C. J., Huterer D., Schwarz D. J., Starkman G. D., 2006, MNRAS, 367, 79

Copi C. J., Huterer D., Schwarz D. J., Starkman G. D., 2013, preprint (arXiv:e-prints)

Cruz M., Martínez-González E., Vielva P., Cayón L., 2005, MNRAS, 356, 29

Cruz M., Martínez-González E., Vielva P., Diego J. M., Hobson M., Turok N., 2008, MNRAS, 390, 913

Das S., Spergel D. N., 2009, Phys. Rev. D, 79, 043007

Driver S. P. et al., 2011, MNRAS, 413, 971

Francis C. L., Peacock J. A., 2010, MNRAS, 406, 14

Garcia-Bellido J., Haugbølle T., 2008, J Cosmol. Astropart. Phys., 4, 3

Gorski K. M., Hivon E., Banday A. J., Wandelt B. D., Hansen F. K., Reinecke M., Bartelmann M., 2005, ApJ, 622, 759

Granett B. R., Neyrinck M. C., Szapudi I., 2008, ApJ, 683, L99

Granett B. R., Neyrinck M. C., Szapudi I., 2009, ApJ, 701, 414

Granett B. R., Szapudi I., Neyrinck M. C., 2010, ApJ, 714, 825

Gurzadyan V. G., Kashin A. L., Khachatryan H., Poghosian E., Sargsyan S., Yegorian G., 2014, A&A, 566, A135

Hambly N. C. et al., 2001, MNRAS, 326, 1279

Inoue K. T., Silk J., 2006, ApJ, 648, 23

Inoue K. T., Silk J., 2007, ApJ, 664, 650

Inoue K. T., Sakai N., Tomita K., 2010, ApJ, 724, 12

Jarrett T. H., Chester T., Cutri R., Schneider S., Skrutskie M., Huchra J. P., 2000, AJ, 119, 2498

Kaiser N., 2004, Proc. SPIE Conf. Ser., SPIE, Bellingham

Keenan R. C., Barger A. J., Cowie L. L., Wang W.-H., Wold I., Trouille L., 2012, ApJ, 754, 131

Kovács A., Szapudi I., 2015, MNRAS, 448, 1305

Kovács A., Szapudi I., Granett B. R., Frei Z., 2013, MNRAS, 431, L28

Kovetz E. D., Kamionkowski M., 2013, Phys. Rev. Lett., 110, 171301

Kron R. G., 1980, ApJS, 43, 305

Land K., Magueijo J., 2005, Phys. Rev. Lett., 95, 071301

Masina I., Notari A., 2009a, J Cosmol. Astropart. Phys., 2, 19

Masina I., Notari A., 2009b, J Cosmol. Astropart. Phys., 7, 35

Masina I., Notari A., 2010, J Cosmol. Astropart. Phys., 9, 28

Ménard B. et al., 2013, preprint (arXiv:e-prints)

Pápai P., Szapudi I., 2010, ApJ, 725, 2078

Pápai P., Szapudi I., Granett B. R., 2011, ApJ, 732, 27

Pedregosa F. et al., 2011, J. Mach. Learn. Res., 12, 2825

Planck Collaboration XXIII, 2014, A&A, 571, A23

Planck Collaboration XXIV, 2014, A&A, 571, A24

Rassat A., Starck J.-L., 2013, A&A, 557, L1

Rassat A., Land K., Lahav O., Abdalla F. B., 2007, MNRAS, 377, 1085

Rassat A., Starck J.-L., Dupé F.-X., 2013, A&A, 557, A32

Rees M. J., Sciama D. W., 1968, Nature, 217, 511

Rubart M., Bacon D., Schwarz D. J., 2014, A&A, 565, A111

Rudnick L., Brown S., Williams L. R., 2007, ApJ, 671, 40

Sachs R. K., Wolfe A. M., 1967, ApJ, 147, L73

Schlegel D. J., Finkbeiner D. P., Davis M., 1998, ApJ, 500, 525

Skrutskie M. F. et al., 2006, AJ, 131, 1163

Smith K. M., Huterer D., 2010, MNRAS, 403, 2

Szapudi I., Prunet S., Colombi S., 2001, ApJ, 561, L11

The Dark Energy Survey Collaboration 2005, preprint (arXiv:e-prints)

Vielva P., 2010, Adv. Astron., 2010, 592094

Vielva P., Martínez-González E., Barreiro R. B., Sanz J. L., Cayón L., 2004, ApJ, 609, 22

Vielva P., Martí Nez -González E., Cruz M., Barreiro R. B., Tucci M., 2011, MNRAS, 410, 33

Wright E. L. et al., 2010, AJ, 140, 1868

Yan L. et al., 2013, AJ, 145, 55

Zhang R., Huterer D., 2010, Astropart. Phys., 33, 69